Locking-free curved elements with refined kinematics for the analysis of composite structures

Locking-free curved elements with refined kinematics for the analysis of composite structures

A.G. de Miguel[*1], G. De Pietro[†1,2], E. Carrera[‡1], G. Giunta[§2], and A. Pagani[¶1]

[1]Department of Mechanical and Aerospace Engineering, Politecnico di Torino, Turin, Italy

[2]Luxembourg Institute of Science and Technology, Esch-sur-Alzette, Luxembourg

[*]Ph.D. Student, alberto.garcia@polito.it

[†]Ph.D. Student, gabriele.depietro@list.lu

[‡]Professor of Aerospace Structures and Aeroelasticity, erasmo.carrera@polito.it

[§]Research Scientist, gaetano.giunta@list.lu

[¶]Assistant Professor, alfonso.pagani@polito.it

Abstract

A new class of refined curved beam elements is proposed for the accurate stress analysis of composite structures. The element possess three-dimensional capabilities and it is suited for the study of curved laminates and fiber-reinforced composites at the microscopic scale. The numerical issues associated with membrane and shear lockings are overcome by means of assumed interpolations of the strain components based on the mixed interpolation of tensorial components method (MITC). Higher-order expansions with only displacement unknowns are employed for the cross-section assumptions at the component level, enabling the computation of component-wise stress fields. For this purpose, a hierarchical set of Legendre functions is implemented, which allows the user to tune the kinematics of the element through the polynomial order input. The detrimental effects of locking in composite modelling are investigated and the robustness and efficiency of the beam element is assessed through comparison against solutions from the literature and refined solid models.

Keywords: MITC, Carrera Unified Formulation, Curved beams, Locking, Micro modelling.

1 Introduction

The confidence in composite structures is growing steadily in the recent years. Their use is extended nowadays to many diverse structural applications and more complex geometries can be produced due to the last advances in composite manufacturing. In order to fully exploit the capabilities of these structures, the simulation community is investing high resources in the development of robust models for the stress analysis of composites at different scales. In this line, the aim of this work is to introduce a new family of curved beam elements with 3D stress capabilities that can reduce substantially the computational costs of composites simulation.

The study of curved geometries increases the complexity of the structural analysis due to the coupling between axial and bending deformations. The first discussions on curved elastic formulations correspond to the early works of Love [**?**] and Lamb [**?**]. Since then, this topic has been discussed vastly in the literature, see for instance Ericksen and Truesdell [**?**], Washizu [**?**], Reissner [**?**], Ashwell and Gallagher [**?**], Banan [**?**] and Tufekci and Arpaci [**?**]. However, it is known that when applying any of these formulations to derive curved beam or shell elements, some severe numerical issues arise that can lead the structural model to fail. In particular, shear locking and membrane locking make the element too stiff when thin structures and curved geometries, respectively, are analyzed. These numerical issues posed one of the major challenges in the finite element method and huge efforts were invested by the structural community to mitigate their detrimental effects. Some of the main contributions are listed in the following. The use of reduced and selective intergration to evaluate the integrals of the troublesome energy terms was done by Noor and Peters [**?**] and Stolarski and Belytschko [**?**]. Dawe [**?**] proposed sets of higher-order polynomials to generete different classes of curved elements for arch problems, showing that a quintic model provides the best results for both thin and thick geometries. A family of locking-free elements was derived based on field-consistent membrane and shear strain interpolations in their constrained physical limits by Babu and Prathap [**?**] and Alturi *et al.* [**?**]. A local penalty-relaxation method was introduced by Tessler and Spiridigliozzi [**?**] in anisoparametric beam elements. Fried [**?**] suggested the generation of the shape functions for curved elements via integrating the assumed polynomial expressions for the strains to avoid the inconsistencies in the strain interpolations. Also, a hybrid-mixed formulation was proposed by Kim and Kim [**?**] in which higher-order interpolation functions are employed to generate elements with nodeless degrees of freedom to mitigate locking.

The present study is devoted to the use of a mixed interpolation of membrane and shear strains to generate refined locking-free curved beam elements. This method, also known as mixed interpolation of tensorial components (MITC), was first introduced by Dvorkin and Bathe [**?**] and MacNeal [**?**] and has proven to be advantageous because it allows to employ a full quadrature in the stiffness matrix components and eliminates the inconsistencies of the interpolation functions for strains and displacements with no need of extra degrees of freedom. For this reason, the MITC method has received much attention in the last decades mainly for

the introduction of locking-free plate and shell elements, see Bucalem and Bathe [**?**], Huang and Hinton [**?**], Park and Stanley [**?**], Jang and Pinsky [**?**] and Cinefra *et al.* [**?**].

This paper presents an extension of MITC to 3D curved beams for composites applications. The aim of this study is twofold: first, thin slender structures and curved geometries are very common in composite applications and limit the use of 3D elements due to the aspect ratio constraints; second, transverse shear and axial terms both play an important role in the behavior of the structure, thus a better approximation of all the tensorial components is required from the simulation. Indeed, the handling of transverse shear strains by means of suitable functions to avoid shear locking was discussed in a previous work by Carrera *et al.* [**?**], who demonstrated the advantages of MITC for the development of robust elements with higher-order models. When dealing with curved geometries, both axial (ε_{ss}) and transverse shear ($\varepsilon_{s\xi}$ and $\varepsilon_{s\eta}$) strains are now assumed by means of reduced-order functions, keeping the element matrices formally the same as those of a standard element.

In order to devise a beam element suitable for composite simulation, some special features must be incorporated in the formulation. Shear deformations and layer-wise mechanics must be incorporated in the theory of structure. Given these difficulties, classical elasticity solutions such as those of Lekhniskii [**?**], Pagano [**?**] or Varadan and Bhaskar [**?**] are still very popular in composite design. Nevertheless, these solutions are limited to simple problems and boundary conditions, therefore there is a continuous need for the development of more accurate models for composites. A comprehensive review of these theories for straigth and curved formulations can be found in Kapania and Ratici [**?**] and Hajianmaleki and Mohamad [**?**]. For laminates, layer-wise models are chosen here to provide highly accurate approximations of strains and stresses over the cross-section. This approach, proposed by Reddy [**?**] and extended in the works of Shimpi and Ghugal [**?**], Tahani [**?**], Ferreira [**?**] and Carrera *et al.* [**?**], among others, is based on the use of independent assumptions of the displacements at each layer. The unified formulation of Carrera [**?**] and a set of Legendre expansions, recently developed by Pagani *et al.* [**?**], are employed to define the kinematics of the beam element in a compact and systematic manner, leaving the order of the theory as a user-defined parameter. For analyses at the microscopic, the component-wise approach is adopted. This theory, proposed by Carrera *et al.* [**?**], is an extension of the layer-wise concept to any component of the composite (e.g. fibres and matrix) over the cross-section of the beam.

The paper is organized as follows. First, the Frenet-Serret framework for curved beams is presented in Section **??**. Section **??** includes the geometrical relations and the constitutive equations of the formulation. The kinematics of the beam element for composite structures is explained in Section **??**, where insights about the layer-wise and component-wise models are provided. The derivation of locking-free curved beam elements based on MITC is presented in Section **??**, and the element arrays and governing equations can be found in Section **??**. The numerical assessment, which includes laminated structures as well as the application to 3D micro models, is shown in Section **??**. Finally, the concluding remarks are drawn in Section **??**.

2 Curved beams: the general framework

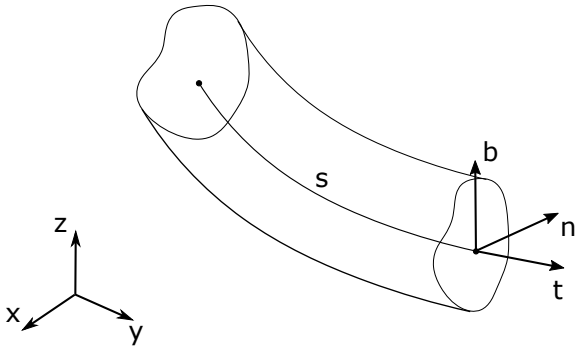

Figure 1: Frenet-Serret coordinate system of a reference beam.

Let us consider a general regular curve represented explicitly by the vector $\mathbf{r}$(s), being s curvilinear abscissa defined along the beam axis. The beam is defined in such a way that the components of $\mathbf{r}(s)$ are the Cartesian coordinates of the line of the centers of the cross-sections along the length of the curve, as shown in Figure **??**. The Frenet-Serret reference frame is defined by a orthonormal vector basis $\{\boldsymbol{t},\boldsymbol{b},\boldsymbol{n}\}$, with:

$$\mathbf{t}(s) = \frac{\frac{d\mathbf{r}(s)}{ds}}{\left\|\frac{d\mathbf{r}(s)}{ds}\right\|}, \qquad \mathbf{n}(s) = \frac{\frac{d^2\mathbf{r}(s)}{ds^2}}{\left\|\frac{d^2\mathbf{r}(s)}{ds^2}\right\|}, \qquad \mathbf{b}(s) = \mathbf{t} \times \mathbf{n}. \tag{1}$$

$\boldsymbol{t}$ is the tangent vector to the curve at abscissa s, $\boldsymbol{n}$ is the normal vector oriented to the inner part of the curve, and $\boldsymbol{b}$ is the binormal vector completing the orthonormal basis. For the sake of convenience, all the problem functions and variables will be expressed in this local frame. The three-dimensional curve can be characterised by two parameters, i.e. curvature κ and torsion τ, respectively:

$$\kappa(s) = \left\|\frac{d^2\mathbf{r}(s)}{ds^2}\right\|, \qquad \tau(s) = \frac{d\mathbf{n}(s)}{ds} \cdot \mathbf{b}. \tag{2}$$

Making use of the Ferret-Serret expressions, the derivatives of the $\{\boldsymbol{t},\boldsymbol{n},\boldsymbol{b}\}$ become:

$$\frac{d}{ds}\begin{Bmatrix}\mathbf{t}\\ \mathbf{n}\\ \mathbf{b}\end{Bmatrix} = \begin{bmatrix}0 & \kappa & 0\\ -\kappa & 0 & \tau\\ 0 & -\tau & 0\end{bmatrix}\begin{Bmatrix}\mathbf{t}\\ \mathbf{n}\\ \mathbf{b}\end{Bmatrix}. \tag{3}$$

In the present formulation, the torsion will not be considered, i.e. $\tau = 0$, that is the beam reference line lies on a plane before deformation.

Let $\{s, \xi, \eta\}$ be the curvilinear coordinates associated to the Frenet-Serret basis. The position of a point P of the beam before deformation can be defined as:

$$\boldsymbol{r}_P = \boldsymbol{r}(s) + \xi\,\boldsymbol{n} + \eta\,\boldsymbol{b}. \tag{4}$$

Subsequently, the determinant of the metric tensor in the aforementioned curvilinear coordinate system writes [**?**]:

$$g = (1 - \kappa\,\xi)^2, \tag{5}$$

and the volume of an infinitesimal parallelepiped within the curved body can be written as

$$dV = \sqrt{g}\,ds\,d\xi\,d\eta. \tag{6}$$

3 Geometrical and constitutive relations

In the proposed framework, the displacement vector of the curved beam can be defined as

$$\mathbf{u} = u_s\mathbf{t} + u_\xi\mathbf{n} + u_\eta\mathbf{b}, \tag{7}$$

or $\mathbf{u} = \{u_s\ u_\xi\ u_\eta\}^T$ in the Frenet-Serret frame. Then, making use of the linear part of the 3D Green-Lagrange equations [**?**], the geometrical relations can be written as:

$$\begin{aligned}
\varepsilon_{ss} &= \frac{1}{H}\left(\frac{\partial u_s}{\partial s} - \kappa u_\xi\right),\\
\varepsilon_{\xi\xi} &= \frac{\partial u_\xi}{\partial \xi},\\
\varepsilon_{\eta\eta} &= \frac{\partial u_\eta}{\partial \eta},\\
\varepsilon_{\xi\eta} &= \frac{\partial u_\xi}{\partial \eta} + \frac{\partial u_\eta}{\partial \xi},\\
\varepsilon_{s\eta} &= \frac{1}{H}\left(\frac{\partial u_\eta}{\partial s}\right) + \frac{\partial u_s}{\partial \eta},\\
\varepsilon_{s\xi} &= \frac{1}{H}\left(\frac{\partial u_\xi}{\partial s} + \kappa u_s\right) + \frac{\partial u_s}{\partial \xi},
\end{aligned} \tag{8}$$

with $H = \sqrt{g}$. At this point, for the purposes of the formulation, it is convenient to write separately the components related to the locking, i.e. axial and shear (ε_{ss}, $\varepsilon_{s\xi}$ and $\varepsilon_{s\eta}$), from those lying on the cross-section, ($\varepsilon_{\xi\xi}$, $\varepsilon_{\eta\eta}$ and $\varepsilon_{\xi\eta}$), as follows:

$$\begin{aligned}
\boldsymbol{\varepsilon}_C &= \{\varepsilon_{ss}\ \ \varepsilon_{s\eta}\ \ \varepsilon_{s\xi}\}^T,\\
\boldsymbol{\varepsilon}_\Omega &= \{\varepsilon_{\xi\xi}\ \ \varepsilon_{\eta\eta}\ \ \varepsilon_{\xi\eta}\}^T.
\end{aligned} \tag{9}$$

It is noteworthy that the deformations of the cross-section in its own plane must be considered, as higher-order theories of structure will be implemented in the kinematics model to account for the transverse deformations. In matrix form, the geometrical relations read:

$$\boldsymbol{\varepsilon}_C = (\boldsymbol{D}_M + \boldsymbol{D}_S)\,\mathbf{u}, \tag{10}$$

$$\boldsymbol{\varepsilon}_\Omega = \boldsymbol{D}_\Omega\,\mathbf{u}, \tag{11}$$

where $\boldsymbol{D}_M$ is the differential operator accounting for the axial terms, $\boldsymbol{D}_S$ is that of the shear terms and $\boldsymbol{D}_\Omega$ is the one for the cross-sectional deformations:

$$\begin{gathered}\boldsymbol{D}_M = \begin{bmatrix} \frac{1}{H}\frac{\partial}{\partial s} & -\frac{1}{H}\kappa & 0 \\ 0 & 0 & 0 \\ \frac{1}{H}\kappa & 0 & 0 \end{bmatrix}, \quad \boldsymbol{D}_S = \begin{bmatrix} 0 & 0 & 0 \\ \frac{\partial}{\partial \eta} & 0 & \frac{1}{H}\frac{\partial}{\partial s} \\ \frac{\partial}{\partial \xi} & \frac{1}{H}\frac{\partial}{\partial s} & 0 \end{bmatrix}, \\ \boldsymbol{D}_\Omega = \begin{bmatrix} 0 & \frac{\partial}{\partial \xi} & 0 \\ 0 & 0 & \frac{\partial}{\partial \eta} \\ 0 & \frac{\partial}{\partial \eta} & \frac{\partial}{\partial \xi} \end{bmatrix}.\end{gathered} \tag{12}$$

Furthermore, it is also convenient to take into account whether these operators act on the longitudinal component of the displacements, or on those lying on the cross-section of the beam. Accordingly, the shear operator becomes:

$$\boldsymbol{D}_S = \boldsymbol{D}_{S_\parallel} + \boldsymbol{D}_{S_\perp}, \tag{13}$$

where

$$\boldsymbol{D}_{S_\parallel} = \begin{bmatrix} 0 & 0 & 0 \\ 0 & 0 & \frac{1}{H}\frac{\partial}{\partial s} \\ 0 & \frac{1}{H}\frac{\partial}{\partial s} & 0 \end{bmatrix}, \quad \boldsymbol{D}_{S_\perp} = \begin{bmatrix} 0 & 0 & 0 \\ \frac{\partial}{\partial \eta} & 0 & 0 \\ \frac{\partial}{\partial \xi} & 0 & 0 \end{bmatrix}. \tag{14}$$

The constitutive laws can be written as:

$$\begin{Bmatrix} \boldsymbol{\sigma}_C \\ \boldsymbol{\sigma}_\Omega \end{Bmatrix} = \begin{bmatrix} \mathbf{C}_{CC} & \mathbf{C}_{C\Omega} \\ \mathbf{C}_{\Omega C} & \mathbf{C}_{\Omega\Omega} \end{bmatrix} \begin{Bmatrix} \boldsymbol{\varepsilon}_C \\ \boldsymbol{\varepsilon}_\Omega \end{Bmatrix}, \tag{15}$$

where $\boldsymbol{\sigma}_C = \{\sigma_{ss}\ \sigma_{s\xi}\ \sigma_{s\eta}\}^T$ includes the axial and shear stresses, and $\boldsymbol{\sigma}_\Omega = \{\sigma_{\xi\xi}\ \sigma_{\eta\eta}\ \sigma_{\xi\eta}\}^T$ includes the transverse and in-plane shear stresses over the cross-section. In the case of an orthotropic material the stiffness matrices, $\mathbf{C}_{CC}$, $\mathbf{C}_{C\Omega}$, $\mathbf{C}_{\Omega C}$ and $\mathbf{C}_{\Omega\Omega}$, write:

$$\begin{gathered}\mathbf{C}_{CC} = \begin{bmatrix} C_{11} & 0 & 0 \\ 0 & C_{55} & 0 \\ 0 & 0 & C_{66} \end{bmatrix}, \quad \mathbf{C}_{\Omega\Omega} = \begin{bmatrix} C_{22} & C_{23} & 0 \\ C_{23} & C_{33} & 0 \\ 0 & 0 & C_{44} \end{bmatrix}, \\ \mathbf{C}_{C\Omega} = \mathbf{C}_{\Omega C}^T = \begin{bmatrix} C_{12} & C_{13} & 0 \\ 0 & 0 & 0 \\ 0 & 0 & 0 \end{bmatrix}.\end{gathered} \tag{16}$$

The expression of the stiffness components C_{ij} in terms of the engineering elastic constants can be found in the books of Reddy [**?**] or Jones [**?**], among others. Moreover, the extension of this formulation to generic anisotropic materials can be done straightforwardly by including the additional terms on these matrices.

4 Unified formulation of composite beams

Towards the enhanced study of composite materials, the kinematics of the MITC beam element is enriched by means of higher-order expansions of the cross-sectional coordinates (ξ, η). Making use of the Carrera's unified formulation of theories of structure (CUF), arbitrary assumptions can be made to capture the deformation of the cross-section of the beam. In this manner, the displacement field can be expressed as:

$$\mathbf{u}(s,\xi,\eta) = F_\tau(\xi,\eta)\mathbf{u}_\tau(s), \qquad \tau = 1,...,M, \tag{17}$$

where $\mathbf{u}_\tau = \{u_{s_\tau} \;\; u_{\xi_\tau} \;\; u_{\eta_\tau}\}^T$ is the generalized displacement vector containing the beam unkwons, F_τ are the assumed functions of the cross-sectional coordinates, and M stands for the total number of assumed functions. The idea is that any complex deformation of the cross-section, and consequently strain and stress fields, can be captured with the use of a proper set of expansion functions, F_τ. For this scope, a hierarchical set of Legendre polynomials is employed in the present study. The proposed theory of structure, denoted to as Hierarchical Legendre Expansions (HLE), was first developed for straight beams by Carrera *et al.* [**?**] using a non-local description of the cross-section surface based on quadrilateral domains. The set of these expansion domains is filled with vertex, side and internal modes, inspired on those developed by Szabó and Babuška [**?**] for the p-version of the FEM. Their expressions are:

- Vertex: included for all polynomial orders, p,

$$F_\tau(\chi,\zeta) = \frac{1}{4}(1-\chi_\tau\chi)(1-\zeta_\tau\zeta), \qquad \tau = 1,2,3,4, \tag{18}$$

- Side: defined for $p \geq 2$,

$$F_\tau(\chi,\zeta) = \frac{1}{2}(1-\zeta)\phi_p(\chi), \qquad \tau = 5,9,13,18,... \tag{19}$$

$$F_\tau(\chi,\zeta) = \frac{1}{2}(1+\chi)\phi_p(\zeta), \qquad \tau = 6,10,14,19,... \tag{20}$$

$$F_\tau(\chi,\zeta) = \frac{1}{2}(1+\zeta)\phi_p(\chi), \qquad \tau = 7,11,15,20,... \tag{21}$$

$$F_\tau(\chi,\zeta) = \frac{1}{2}(1-\chi)\phi_p(\zeta), \qquad \tau = 8,14,16,21,..., \tag{22}$$

- Internal: introduced for $p \geq 4$,

$$F_\tau(\chi,\zeta) = \phi_{p_1}(\chi)\phi_{p_2}(\zeta), \qquad p = p_1 + p_2, \tag{23}$$

where χ and ζ vary over the natural domain between -1 and $+1$, and ϕ_p are the 1D Legendre-type internal polynomials defined in [**?**] or [**?**].

The main advantages of HLE theories is that once the cross-section domain is defined, the accuracy of the model is tuned through the order of the polynomial expansions F_τ, which

remains as an input of the analysis. Another interesting feature is the possibility of mapping different geometries into the quadrilateral domains in a non-isoparametric sense, which allows the user to represent the exact shape of all the components of the composite structure. More details about this technique are provided the work of Carrera *et al.* [**?**]. In this work, layer-wise and component-wise models are generated on the basis of HLE.

4.1 Layer-wise and component-wise models

In layer-wise models, each layer of the composite is allowed to deform independently and the compatibility conditions are imposed at the interfaces between two successive plies. In the unified framework, the kinematics of the beam element, Eq. (**??**), becomes:

$$\mathbf{u}(s,\xi,\eta) = F_\tau^k(\xi,\eta)\mathbf{u}_\tau^k(s), \qquad \tau = 1, ..., M, \tag{24}$$

where the index k accounts for the layer numbering. In this manner, a set of F_τ^k expansion functions is generated for layer k-th and the compatibility is assured in the assembly of the stiffness matrix,

$$\mathbf{u}_{top}^k = \mathbf{u}_{bottom}^{k+1}, \tag{25}$$

as shown on the left-hand side of Fig. **??**. This model was originally introduced using HLE theories by Pagani *et al.* [**?**] for the analysis of classical laminates and thin-walled composite structures.

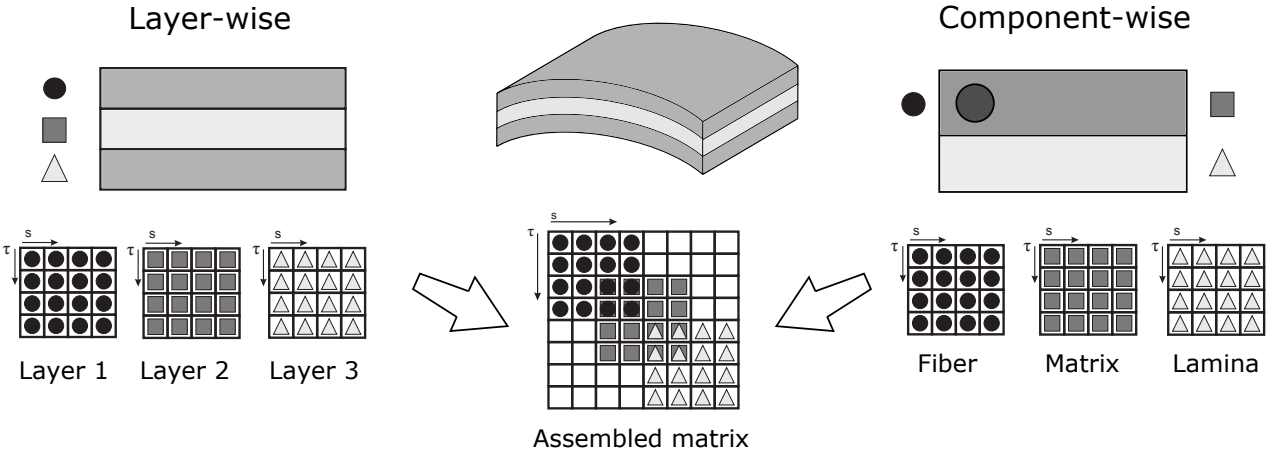

Figure 2: Comparison of the layer-wise and component-wise formal approaches in composite analysis.

Based on this approach and exploiting the capabilities of the unified formulation, a generalization of the layer-wise approach to any component over the cross-section can be straightforwardly devised. In fact, by only extending the meaning of the index k from the layer to generic constituents, one can generate independent kinematics for the fibers, matrix or any other component, and impose the compatibility of the displacements at their interfaces in the cross-section domain. Subsequently, the assembly procedure of the kinematics of each

component into the stiffness matrix of the element remains formally the same as that of layer-wise approaches, as illustrated on the right-hand side of Fig. **??**. The use of HLE theories of structure in a component-wise sense was introduced by Carrera *et al.* [**?**] for the analysis of 3D microscopic models. The enrichment of the element kinematics using layer-wise or component-wise models is crucial for the accurate stress analysis of composite structures, where classical theories fail. For the sake of clarity, the use of the index k will be avoided in the following, with no generality lost in the formulation.

5 Curved beam elements based on MITC

When formulating standard displacement-based beam elements, the nodal unknowns are interpolated over the beam axis using a certain polynomial base, N_i. In the CUF framework for beams, the generalised displacements over the finite element space can be written as:

$$\mathbf{u}_\tau(s) = N_i(s)\mathbf{u}_{\tau i} \qquad\qquad i = 1, ..., N_{node}, \tag{26}$$

where $\boldsymbol{u}_{\tau i} = \{u_{s_{\tau i}} \; u_{\xi_{\tau i}} \; u_{\eta_{\tau i}}\}^T$ are the nodal unknowns and N_{node} stands for the total number of nodes in the element. In the present work, a Lagrange-based polynomial set is employed to generate equispaced 2-node linear (B2), 3-node quadratic (B3) and 4-node cubic (B4) beam elements. The explicit expressions of these interpolating functions can be found in the book of Bathe [**?**].

Using Eqs. (**??**) and (**??**), the strains of the standard element can be written in the form of Eq. (**??**) as

$$\boldsymbol{\varepsilon}_C = F_\tau(\boldsymbol{D}_M N_i\mathbf{I})\mathbf{u}_{\tau i} \; + \; F_\tau(\boldsymbol{D}_{S_\parallel} N_i\mathbf{I})\mathbf{u}_{\tau i} \; + \; (\boldsymbol{D}_{S_\perp} F_\tau\mathbf{I})N_i\mathbf{u}_{\tau i}, \tag{27}$$

$$\boldsymbol{\varepsilon}_\Omega = (\boldsymbol{D}_\Omega F_\tau\mathbf{I})N_i\mathbf{u}_{\tau i} \; , \tag{28}$$

where $\mathbf{I}$ is the 3×3 identity matrix.

The effects of shear locking in thin finite elements have received wide attention since the introduction of FEM and were already addressed in [**?**]. However, when curved geometries are considered, the axial strains associated to the curvature terms can lead also to an increase of the bending stiffness [**?**]. This numerical issue, commonly known as membrane locking, is caused by inconsistencies in the interpolations of the strains due to the curvature terms and can have detrimental effects in the performance of the finite element. In order to solve this issue and to overcome all kinds of locking, the axial and shear strains can be reformulated as follows:

$$\bar{\boldsymbol{\varepsilon}}_C = \bar{N}_m \, \boldsymbol{\varepsilon}_{C_m} \qquad m = 1, ..., n_{node} - 1, \tag{29}$$

where $\bar{\boldsymbol{\varepsilon}}_C$ are the assumed axial and shear strains. In this manner, these components are approximated using a lower-order set of functions, $\bar{N}_m$, that interpolate the strains obtained from the displacements, ε_{C_m}, at certain points along the length of the element, which are called

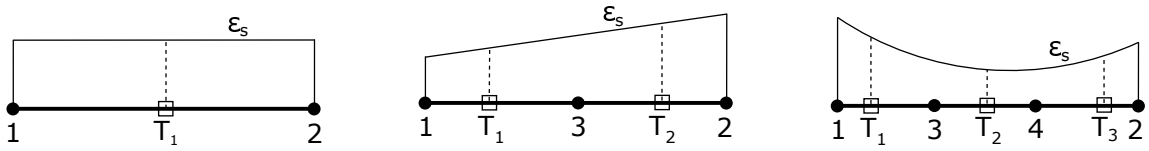

(a) 2-node (b) 3-node (c) 4-node

Figure 3: Assumed strains in MITC beam elements and tying points.

tying points. The tying points, hereinafter T_m, are shown in Fig. **??** and their locations for linear, quadratic and cubic beam elements are:

$$\begin{aligned} B2: &\qquad r_{T_1} = 0, \\ B3: &\qquad r_{T_1} = -\tfrac{1}{\sqrt{3}},\ r_{T_2} = \tfrac{1}{\sqrt{3}}, \\ B4: &\qquad r_{T_1} = -\sqrt{\tfrac{3}{5}},\ r_{T_2} = 0,\ r_{T_3} = \sqrt{\tfrac{3}{5}}\ , \end{aligned} \tag{30}$$

where r is the coordinate in the natural frame of the beam element. These points, also known as Barlow points, provide the best strain values within the element and, in most cases, coincide with the Gauss points [**?**]. For the sake of completeness, the set of assumed functions employed in the present formulation is provided in Appendix **??**.

Evaluating the strains of Eq. (**??**) by means of Eq. (**??**), the vector containing the axial and shear terms becomes:

$$\bar{\boldsymbol{\varepsilon}}_C = \bar{N}_m F_\tau (\boldsymbol{D}_M N_i \mathbf{I})_m \mathbf{u}_{\tau i} \ + \ \bar{N}_m F_\tau (\boldsymbol{D}_{S_\parallel} N_i \mathbf{I})_m \mathbf{u}_{\tau i} \ + \ \bar{N}_m (\boldsymbol{D}_{S_\perp} F_\tau \mathbf{I}) N_{i_m} \mathbf{u}_{\tau i}\ , \tag{31}$$

where the subscript m denotes evaluation of the standard shape functions and their derivatives at the tying points, except for $\bar{N}_m$.

Finally, according to the constitutive relations of Eq. (**??**), the stresses can be written as:

$$\begin{aligned} \bar{\boldsymbol{\sigma}}_C = \ & \mathbf{C}_{CC} \left[\bar{N}_m F_\tau (\boldsymbol{D}_M N_i \mathbf{I})_m \mathbf{u}_{\tau i} \ + \ \bar{N}_m F_\tau (\boldsymbol{D}_{S_\parallel} N_i \mathbf{I})_m \mathbf{u}_{\tau i} \right. \\ & \left. + \bar{N}_m (\boldsymbol{D}_{S_\perp} F_\tau \mathbf{I}) N_{i_m} \mathbf{u}_{\tau i} \right] + \ \mathbf{C}_{C\Omega} \left[(\boldsymbol{D}_\Omega F_\tau \mathbf{I}) N_i \mathbf{u}_{\tau i} \right], \\ \bar{\boldsymbol{\sigma}}_\Omega = \ & \mathbf{C}_{\Omega C} \left[\bar{N}_m F_\tau (\boldsymbol{D}_M N_i \mathbf{I})_m \mathbf{u}_{\tau i} \ + \ \bar{N}_m F_\tau (\boldsymbol{D}_{S_\parallel} N_i \mathbf{I})_m \mathbf{u}_{\tau i} \right. \\ & \left. + \bar{N}_m (\boldsymbol{D}_{S_\perp} F_\tau \mathbf{I}) N_{i_m} \mathbf{u}_{\tau i} \right] + \ \mathbf{C}_{\Omega\Omega} \left[(\boldsymbol{D}_\Omega F_\tau \mathbf{I}) N_i \mathbf{u}_{\tau i} \right]. \end{aligned} \tag{32}$$

6 Governing equations

The governing equations are obtained through the principle of virtual displacements (PVD). The variation of the virtual internal work, δL_{int}, includes the contribution of the membrane and shear strains, δL_{int_C}, and the sectional strains, δL_{int_Ω}. Making use of Eq. (**??**), these

terms are:

$$\delta L_{int_C} = \int_l \int_{Sect} \delta\bar{\boldsymbol{\varepsilon}}_C^T \, \bar{\boldsymbol{\sigma}}_C \, H d\Omega \, ds = \int_l \int_{Sect} (\delta\bar{\boldsymbol{\varepsilon}}_C^T \, \bar{\boldsymbol{C}}_{CC} \, \bar{\boldsymbol{\varepsilon}}_C \; + \; \delta\bar{\boldsymbol{\varepsilon}}_C^T \, \bar{\boldsymbol{C}}_{C\Omega} \, \boldsymbol{\varepsilon}_\Omega) \, H d\Omega \, ds, \tag{33}$$

$$\delta L_{int_\Omega} = \int_l \int_{Sect} \delta\boldsymbol{\varepsilon}_\Omega^T \, \bar{\boldsymbol{\sigma}}_\Omega \, H d\Omega \, ds = \int_l \int_{Sect} (\delta\boldsymbol{\varepsilon}_\Omega^T \, \bar{\boldsymbol{C}}_{\Omega C} \, \bar{\boldsymbol{\varepsilon}}_C \; + \; \delta\boldsymbol{\varepsilon}_\Omega^T \, \bar{\boldsymbol{C}}_{\Omega\Omega} \, \boldsymbol{\varepsilon}_\Omega) H \, d\Omega \, ds, \tag{34}$$

where l is the length of the beam and $Sect$ is the total surface of the cross-section. Considering Eq. (**??**) and (**??**), the internal work can be written in a compact manner as:

$$\delta L_{\text{int}} = \delta L_{int_C} + \delta L_{int_\Omega} = \delta \mathbf{u}_{\tau i}^T (\, \mathbf{K}_{CC}^{\tau\varsigma ij} + \mathbf{K}_{C\Omega}^{\tau\varsigma ij} + \mathbf{K}_{\Omega C}^{\tau\varsigma ij} + \mathbf{K}_{\Omega\Omega}^{\tau\varsigma ij} \,) \mathbf{u}_{\varsigma j} \; , \tag{35}$$

where the $\mathbf{K}^{\tau\varsigma ij}$ matrices are the fundamental nuclei of the stiffness matrix. They contain the integrals of the expansion functions, indicated by the indexes τ and ς, and those of the 1D interpolating functions, indicated by i and j. The explicit form of the components of the fundamental nuclei is provided in Appendix **??**. One can notice that, in the unified framework, any theory of structure, e.g. layer-wise or component-wise, can be formulated into the element in terms of these fundamental nuclei with an appropriate number of expansion terms, which is selected by the user as an input.

Using the same notation, the virtual external work for a generic point load $\boldsymbol{P}_{\tau i} = (P_{s_{\tau i}} \, P_{\xi_{\tau i}} \, P_{\eta_{\tau i}})$ reads:

$$\delta L_{\text{ext}} = \delta \boldsymbol{u}_{\tau i}^T \, \boldsymbol{P}_{\tau i} \; . \tag{36}$$

The formulation of generic pressure loads is shown in [**?**].

Considering the equivalence of virtual works,

$$\delta L_{\text{int}} = \delta L_{\text{ext}}, \tag{37}$$

the governing equations read:

$$\delta \boldsymbol{u}_{\tau i} : \qquad \boldsymbol{K}^{\tau\varsigma ij} \, \boldsymbol{u}_{\varsigma j} = \boldsymbol{P}_{\tau i} \; , \tag{38}$$

where $K^{\tau\varsigma ij}$ is the total sum of the fundamental nuclei of Eq. (**??**).

The element here proposed includes some interesting features for the analysis of composite structures. First, it does not lock and provides a better approximation of the axial and shear stresses along the beam axis without adding extra degrees of freedom. It also avoids the appearance of unexpected spurious modes, which occur when other well-known numerical artefacts are employed [**?**], such as the reduced integration. In addition, the use of layer-wise/component-wise kinematics for the cross-sectional assumptions enables the representation of the different constituents for laminated structures and multi-component composites, while keeping the computational advantages of beam formulations.

7 Numerical examples

Several numerical analyses are proposed in this section to show the advantages of refined curved beam elements based on MITC. First, a locking assessment is performed accounting for different meshes and slenderness ratios. In a second case, the capabilities of refined layer-wise elements for the accurate stress analysis is proven through a benchmark case of a circular laminated disk. Finally, a 3D microstructure is analyzed using the component-wise approach and the efficiency of the model is demonstrated against solid models.

7.1 Locking analysis

The performance of MITC beam elements to mitigate shear and membrane locking in curved geometries is demonstrated as a first assessment. A simply-supported laminated beam is considered and the focus is on the effect of the slenderness ratio and the polynomial order of the shape functions of the element. The geometry of the problem is shown in Figure **??**. The section is rectangular, being the total height, h, equal to 0.6 m, and the total width, b, equal to 0.4 m. The opening angle is $\Phi = 2/3\pi$ and two different slenderness ratios are studied, namely $L/h = 5$ and $L/h = 500$, accounting for a thick and a very slender beam. Two layers of equal thickness are considered in the radial direction and modelled as a layer-wise expansion over (ξ, η) using first-order Legendre polynomials, hereinafter referred to as 2HL1. The material properties of each layer are listed in Table **??**.

	E_1 (GPa)	E_2, E_3 (GPa)	G_{12}, G_{13}, G_{23} (GPa)	ν_{12}, ν_{13}, ν_{23}
material 1	30	1	0.5	0.25
material 2	5	1	0.5	0.25

Table 1: Material properties of the two-layer arc. The index 1 refers to the axial direction, whereas 2 and 3 correspond to the normal and bi-normal directions, respectively.

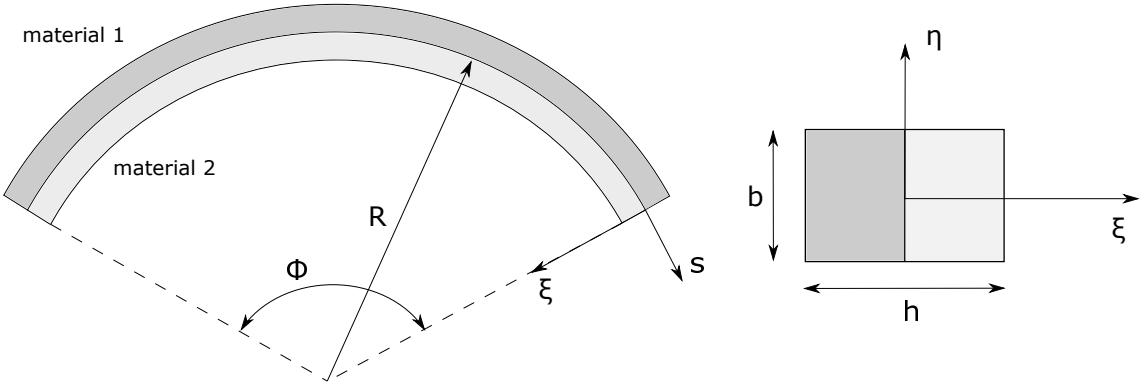

Figure 4: Geometry and section of the arc used for the locking assessment.

Navier-type exact solutions are used as references in all cases. The derivation of strong form solutions for refined beam models is presented in the companion paper [**?**]. A point

force of magnitude $P = 1000$ N is applied at midspan in $\xi = 0.0$ and $\eta = 0.0$. The analytical solutions for the radial displacement at the center of the beam are $u_\xi^{Nav} = 4.735 \times 10^{-5}$ m for $L/h = 5$ and $u_\xi^{Nav} = 23.169$ m for $L/h = 500$. Figures **??**, **??** and **??** show the normalized radial displacements $\bar{u}_\xi = u_\xi / u_\xi^{Nav}$ for an increasing number of beam elements, N, featuring two, three and four nodes, respectively. The graphs include the solutions of elements using full integration schemes (B*) against those obtained from MITC beam elements (MITC*). From these results, it is possible to conclude that:

- Analytical Navier-type solutions represent an exact solution in the framework of the proposed formulation and, therefore, represent the best assessment to evaluate the locking correction method. Reference results are herein obtained using 200 half waves.

- Locking is more evident for lower order elements and have disastrous effects on slender structures. The use of higher-order shape functions alleviates to some extent the problem, although the computational size of the model increases. In view of this results, third-order elements are employed hereinafter.

- The MITC element avoids locking independently of the slenderness ratio, see Fig. **??**. The convergence rates shown by the element are also superior to those of standard beam elements, which leads to a more efficient analysis.

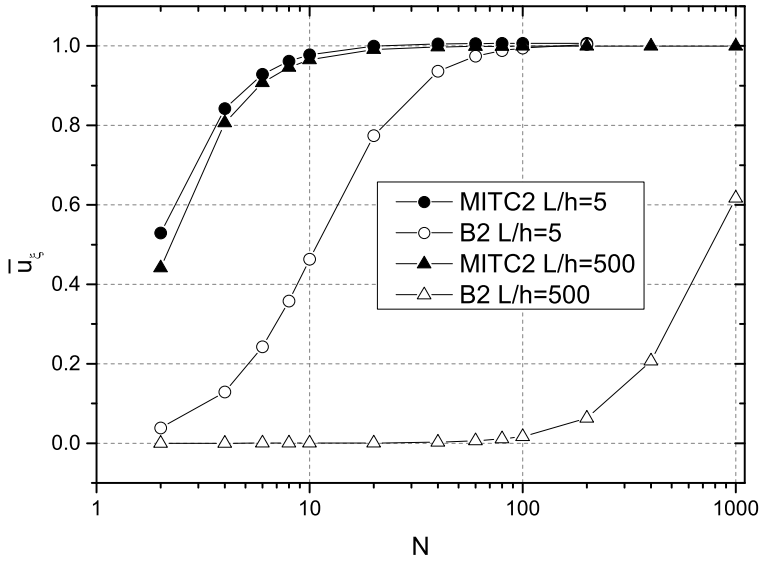

Figure 5: Radial displacement, $\bar{u}_\xi$, at midspan for an increasing number of 2-node curved elements. Slenderness ratios $L/h = 5$ and $L/h = 500$.

7.2 Laminated circular disk

A circular laminate is considered as a second numerical example to assess the stress accuracy of the element. It consists in a benchmark hollow cylindrical disk with internal pressure, see Fig. **??** (a). This problem was studied by Surana and Nguyen [**?**] and analytical solutions

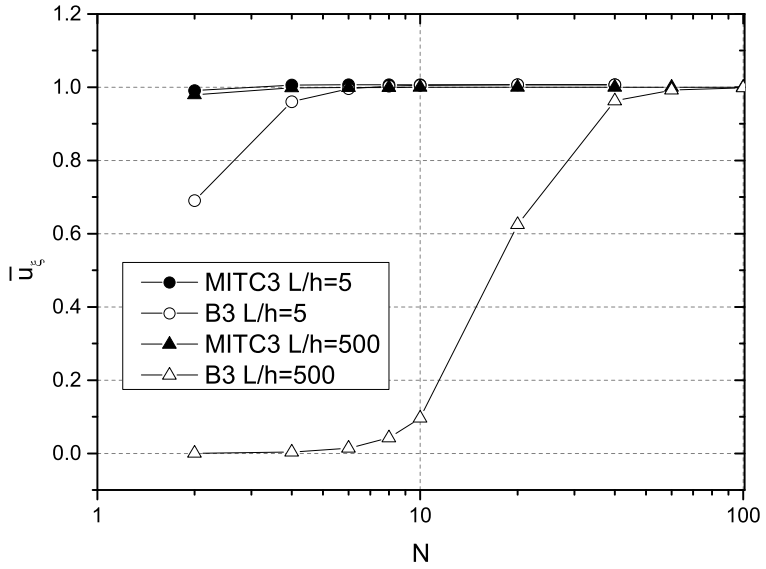

Figure 6: Radial displacement, $\bar{u}_\xi$, at midspan for an increasing number of 3-node curved elements. Slenderness ratios $L/h = 5$ and $L/h = 500$.

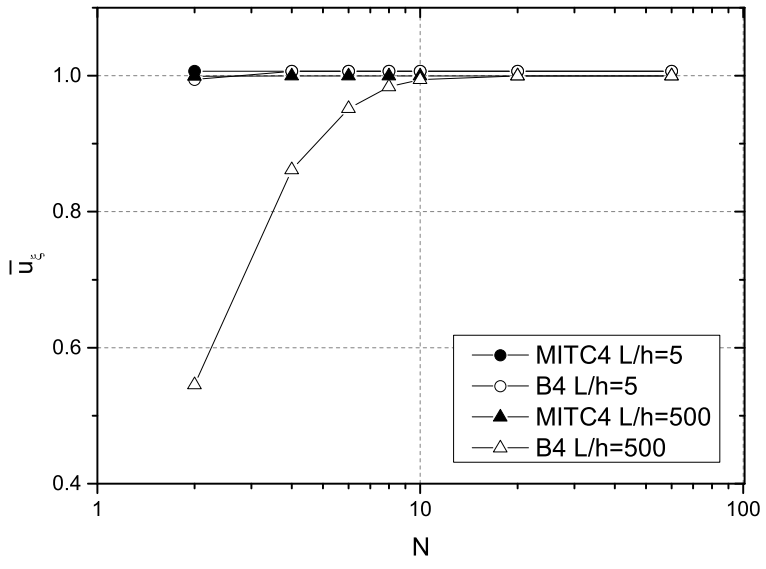

Figure 7: Radial displacement, $\bar{u}_\xi$, at midspan for an increasing number of 4-node curved elements. Slenderness ratios $L/h = 5$ and $L/h = 500$.

from Lekhnitskii [**?**] are available. In order to be consistent with the references, plane stress assumptions are applied and no units are provided, therefore no conversion is performed in the computations. The laminate is made of a stack of eight layers of two different materials with the following elastic properties:

$$\begin{aligned} &material\ 1: \quad E_1/E_2 = 30,\ G_{12}/E_2 = 0.5,\ \nu_{12} = 0.25 \\ &material\ 2: \quad E_1/E_2 = 5,\ G_{12}/E_2 = 0.5,\ \nu_{12} = 0.25 \end{aligned} \tag{39}$$

for $E_2 = 1 \times 10^6$. The radius of the center line of the structure, R, is equal to 10, and the total thickness, h, is equal to 8. The value of the pressure, P, applied at the inner wall is 1000. Given the double symmetry of the problem, only a quarter of the structure is modelled. The beam model proposed is presented in Fig. **??** (b). It accounts for 4 curved MITC beam elements and a layer-wise distribution of the unknowns based on HLE.

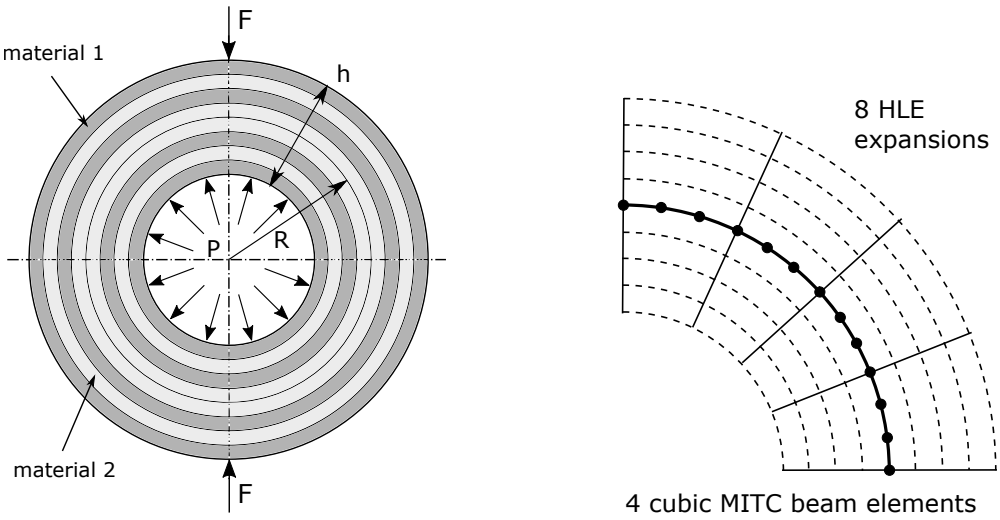

(a) Case (b) Refined beam model

Figure 8: Features of the hollow laminated ring case and proposed refined beam model.

Figures **??**, **??** and **??** show the distributions of radial displacements, radial stresses and circumferential stresses, respectively, versus the thickness coordinate in radial direction. Exploiting the capabilities of HLE theories of structure, several polynomial degrees are evaluated at the layer-level and compared with the solutions from [**?**]. In the latter work, a two-dimensional formulation of curved beams is developed using higher-order Lagrangian polynomials for the displacements over the whole thickness in an equivalent single layer (ESL) approach. Subsequently, the authors discretize the center line with a total of 45 quadratic beam elements and convergence to the analytical solutions is achieved by increasing the polynomial degree of the assumed functions, p. In the graphs, the LW solutions obtained with MITC elements are labeled as HL1 to HL8, standing for first to eight polynomial degree; and the results from [**?**] are referred to as $p = 1$ to $p = 4$. The analytical solutions based on [**?**] are also included as references. Finally, Fig. **??** shows the plot of the stress solutions over the disk for the HL3 model.

Although, in general, ESL models are computationally less expensive in comparison to LW models, their convergence is much slower and very high polynomial orders are required to obtain accurate solutions in laminated structures, as shown in Fig. **??**. It is possible to observe that the HL2 model is already in good agreement with the analytical solution, whereas the forth order, $p = 4$, still oscillates around it. Regarding the radial stresses, displacement-based LW solutions do not necessary satisfy the equilibrium conditions at the interfaces, although a third-order expansion (HL3) provides almost continuous solutions.

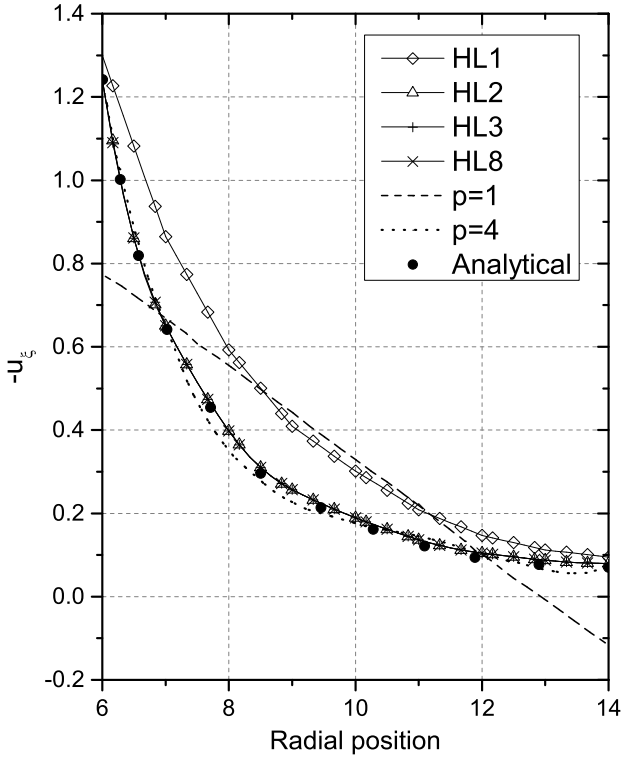

Figure 9: Radial displacement, u_ξ, through the thickness of the laminated disk.

To complete the analysis of the laminated disk, a second load case is herein considered. The structure is now pinched with two opposite and equal loads, F, acting on the top and bottom points, as shown in Fig. **??** (a). The magnitude of these forces is $F = 5$. Table **??** includes a comparison between the solutions of radial displacements and stress solutions obtained from standard full integrated elements and MITC elements. In order to show the influence of the slenderness ratio and the locking effects in all the solutions, two radius are proposed, which are $R = 10$ and $R = 500$. One can notice that for the thick disk, the local effects around the loaded region play a major role and no convergence is observed for u_ξ and σ_{ss}. Also, both integration schemes behave similarly. On the other hand, for high slenderness ratios, the membrane effects become more important and MITC beam elements show their superiority, both in terms of displacements and stresses.

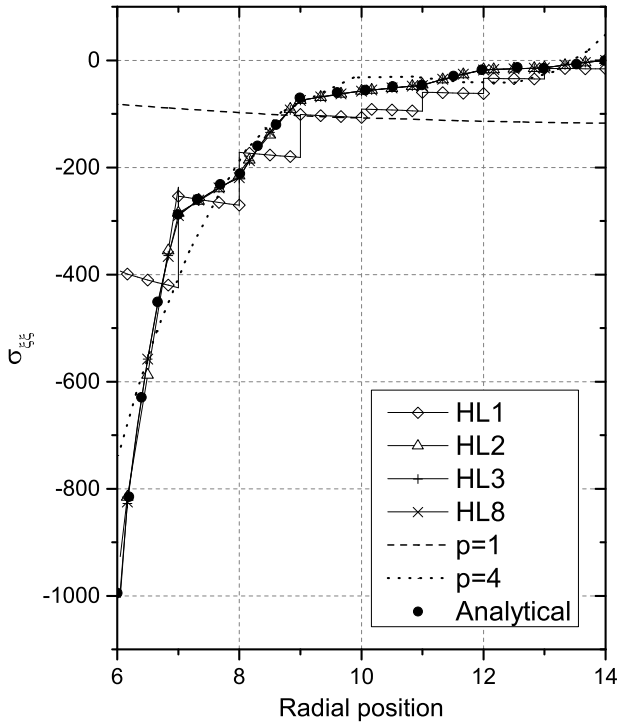

Figure 10: Radial stress, $\sigma_{\xi\xi}$, through the thickness of the laminated disk.

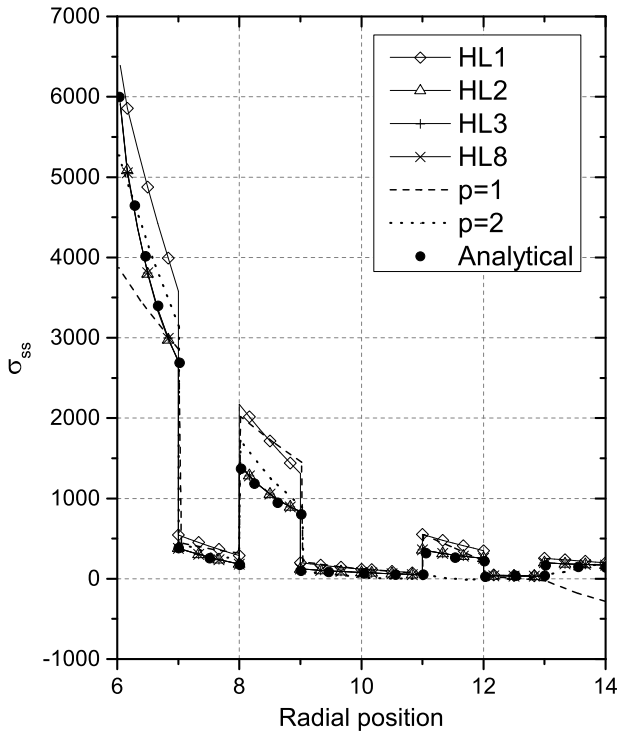

Figure 11: Circumferential stress, σ_{ss}, through the thickness of the laminated disk.

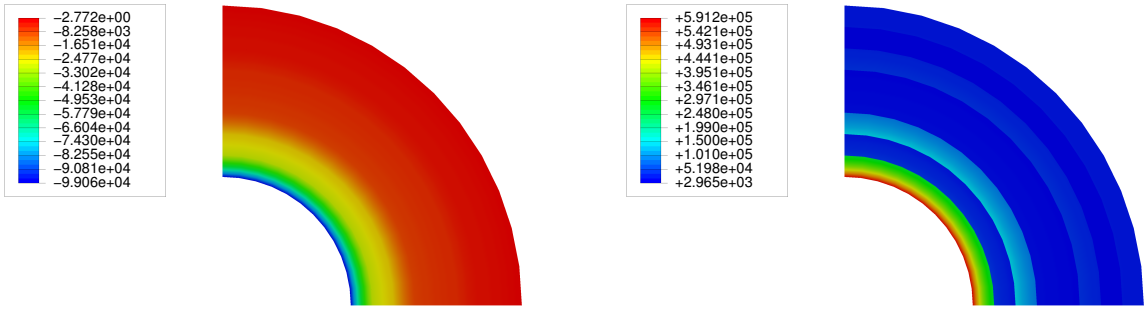

(a) Radial stress (b) Circumferential stress

Figure 12: Stress fields over the eight-layer curved beam for the third order HL3 model.

7.3 3D microstructure

The last numerical case deals with a 3D micro model of a fiber-matrix arrangement. The study focuses on the use of the proposed locking-free beam elements as a high-fidelity low-cost tool for the stress analysis of complex composite problems. The geometrical features of the model are shown in Fig. **??**. The configuration recalls a typical case of curved fibers that are prone to fail due to kinking. The mechanical properties of the materials are those of a IM7/8551-7 carbon/epoxy composite, see Table **??**. A fiber volume fraction of 0.5027 is considered. The opening angle of the structure is equal to a quarter of a circle and two fibers are included in the model. Simply supported conditions are applied at both the edges, i.e. $u_\xi = u_\eta = 0$ for $s = (0, L)$, and the symmetry is imposed at the center of the microstructure, i.e. $u_s = 0$ at $s = L/2$. The loading configuration proposed is a pull-out of the fibers of a magnitude of 1 N at each edge, modelled as a distributed pressure over the section of the fibers.

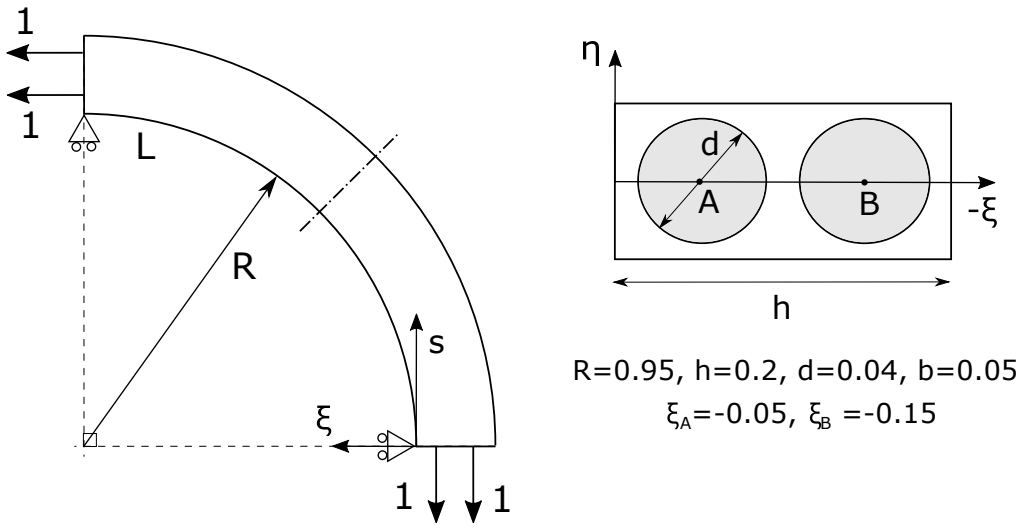

Figure 13: Geometry and section of the fiber-matrix microstructure. Distances in mm and forces in N.

A convergence analysis is performed for both the mesh of MITC curved elements and

R=10	$u_\xi \times 10^3$ [L,-h/2,0]		$\sigma_{ss} \times 10^{-3}$ [L,-h/2,0]		$\sigma_{\xi\xi} \times 10^{-1}$ [0,0,0]		$\sigma_{s\xi} \times 10^{-1}$ [L/2,0,0]		DOFs
No. B4	MITC	Full	MITC	Full	MITC	Full	MITC	Full	
1	3.535	3.370	-2.645	-3.169	-2.280	-4.477	11.917	11.490	816
2	4.184	4.122	-5.019	-5.497	-2.187	-2.271	7.182	7.832	1428
3	4.553	4.516	-6.936	-7.417	2.262	-2.271	10.713	10.682	2040
4	4.811	4.786	-8.553	-9.087	-2.265	-2.268	9.813	9.832	2652
10	5.615	5.610	-14.337	-15.253	-2.266	-2.266	9.845	9.845	6324
R=500	$u_\xi \times 10^{-1}$ [L,-h/2,0]		$\sigma_{ss} \times 10^{-4}$ [L,-h/2,0]		$\sigma_{\xi\xi} \times 10^{-1}$ [0,0,0]		$\sigma_{s\xi} \times 10^{-2}$ [L/2,0,0]		DOFs
No. B4	MITC	Full	MITC	Full	MITC	Full	MITC	Full	
1	1.962	0.072	-4.151	0.294	-6.449	0.053	1.518	-0.714	816
2	1.970	1.520	-4.047	-1.212	-6.404	-8.196	1.104	6.431	1428
3	1.970	1.882	-4.037	-2.845	-6.327	-7.419	1.328	4.436	2040
4	1.969	1.950	-4.038	-3.528	-6.326	-6.872	1.286	1.957	2652
10	1.970	1.970	-4.068	-4.025	-6.329	-6.352	1.230	1.233	6324

Table 2: Displacements and stress solutions of the pinched laminated disk for two different radius. The number of degrees of freedom (DOFs) corresponds to the maximum number of unknowns of the linear problem.

	E_1 (GPa)	E_2, E_3 (GPa)	G_{12}, G_{13} (GPa)	G_{23} (GPa)	ν_{12}, ν_{13}	ν_{23}
IM7 fiber	276	19	27	7	0.2	0.2
8551-7 matrix	4.08	4.08	1.478	1.478	0.38	0.38

Table 3: Material properties of the carbon fiber and epoxy matrix used for 3D microstructure, obtained from Kaddour and Hinton [**?**].

a solid model generated in the commercial software ABAQUS using linear C3D8 elements. The curved MITC elements here proposed are generated using a distribution of HLE expansions of fourth order (HL4) over the cross-section, which are capable of representing the exact geometry of the constituents in a component-wise sense. More details of the modeling procedure are provided in Carrera *et al.* [**?**]. Table **??** shows the maximum deflection of the structure for all the models generated. Three different solid models were generated with increasing mesh refinements. One can notice that in solid modeling, in order to capture the actual deformation of the structure, a very refined mesh is needed to represent accurately the total volume and the correct ratio between the constituents. On the other hand, the curved beam elements keep always the actual geometry of the cross-section, therefore convergence is reached faster. Figure **??** shows a comparison of the displacement results and the model's geometrical features.

Finally, Fig. **??**, **??** and **??** show the longitudinal, radial and transverse shear stress fields over the fibers for the two approaches. It is clear that both approaches are in high agreement both in terms of magnitude and distribution of the solutions. These results illustrate the actual

MITC beam - HL4					
mesh	2 B2 (1,413)	2 B3 (2,355)	2 B4 (3,297)	4 B4 (6,123)	14 B4 (20,253)
$u_{max} \times 10^5$	2.775	4.918	4.940	4.942	4.942
ABAQUS - C3D8					
mesh	(54,417)	(245,979)	(575,667)		
$u_{max} \times 10^5$	5.150	5.115	4.965		

Table 4: Maximum deflection in magnitude, u_{max}, of the fiber-matrix micro model. Number of degrees of freedom between parentheses.

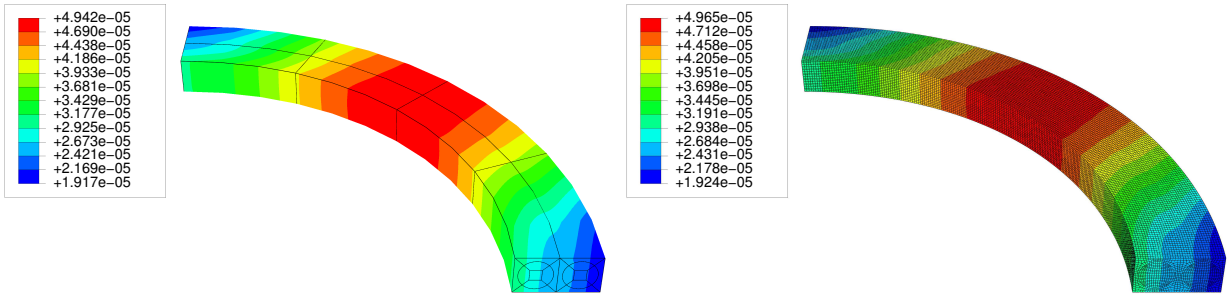

(a) MITC4-HL4 (b) ABAQUS

Figure 14: Comparison of displacement resultant (m) and modeling procedure.

potential of MITC beam models for the study of composite materials. The computational costs of problems such this one usually remains as a limiting factor in composite analysis and compromises the accuracy of the stress solutions. In this regard, the use of a proper beam element with enhanced kinematics over the cross-section can be used to reduce the size of the computational problem by orders of magnitude with no loss of accuracy. The low levels of bandwidth in the stiffness matrix of CUF beam models also promotes less computational costs when compared with 3D FEM models.

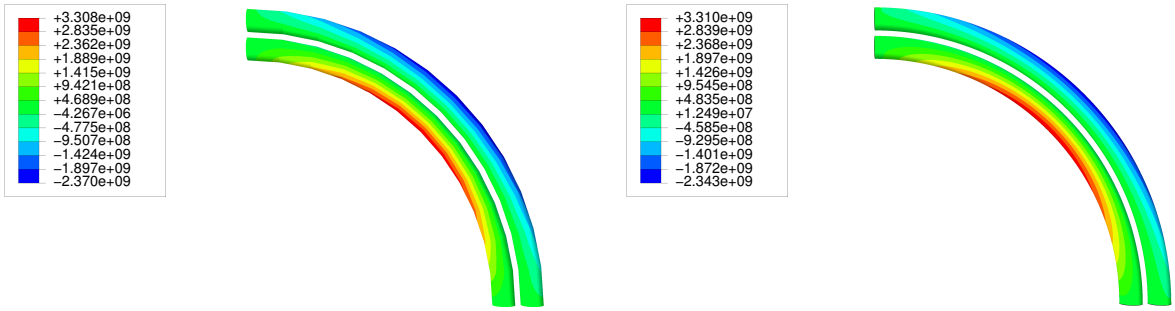

(a) MITC4-HL4 (b) ABAQUS

Figure 15: Longitudinal stresses (Pa) over the fibers of the micro model.

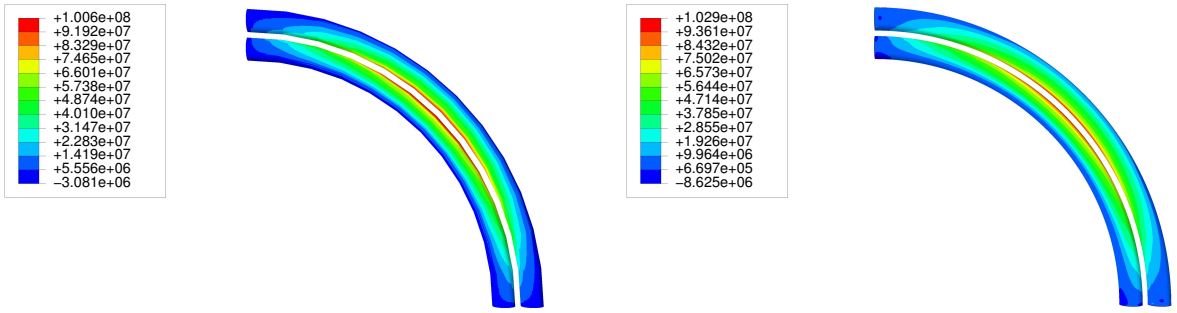

(a) MITC4-HL4 (b) ABAQUS

Figure 16: Radial stresses (Pa) over the fibers of the micro model.

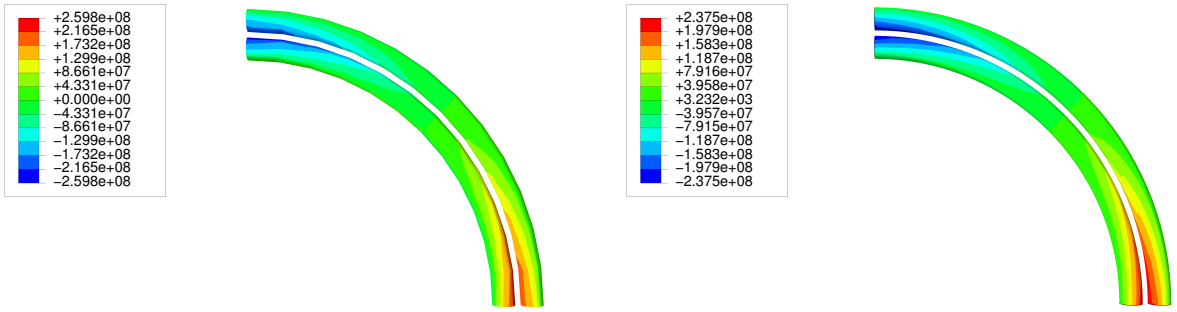

(a) MITC4-HL4 (b) ABAQUS

Figure 17: Shear stresses, $\sigma_{s\xi}$, (Pa) over the fibers of the micro model.

8 Conclusions

This paper introduces a novel family of locking-free beam elements with component-wise capabilities that possesses great advantages for the analysis of composite structures. The use of the MITC method is twofold: first, the membrane and shear locking is eliminated in a natural manner, and also, it allows a better representation of the strain and stress solutions in comparison to standard integration schemes. From the results of this study, the authors conclude that:

- Membrane and shear locking are completely mitigated and convergence rates of the beam model are clearly improved, especially for thin structures, which are typical in composite applications.
- The fidelity of the stress solutions is proven through comparison against analytical solutions of benchmark problems and highly refined 3D models.
- The element is proposed for the accurate analysis of composite materials at different scales, from the structural modeling to the micromechanics, due to its robustness, efficiency and straightforward implementation in a FEM framework.

The potential of the CW formulation extends to the damage and failure study of composite structures, in which the computation of accurate 3D stress fields is of paramount importance

and the computational costs remains as a limiting factor of the analysis. Future investigations will be dedicated to more realistic applications of aerospace thin-walled structures and local effects at the micro-scale, such as fiber kinking.

Acknowledgments

This research has been funded by the Marie Sklodowska-Curie action grant agreement no. 642121, as part of the FULLCOMP project. The European Commission is gratefully acknowledged. A. Pagani also acknowledges financial support from the Compagnia di San Paolo trough the project ADAMUS.

A Assumed functions for axial and shear strains

The interpolating functions of the assumed strains, $\bar{N}_m$, for linear, quadratic and cubic beam elements are:

$$
\begin{aligned}
&B2: && \bar{N}_1 = 1, \\
&B3: && \bar{N}_1 = -\tfrac{1}{2}\sqrt{3}(\xi - \tfrac{1}{\sqrt{3}}), \quad \bar{N}_2 = \tfrac{1}{2}\sqrt{3}(\xi + \tfrac{1}{\sqrt{3}}), \\
&B4: && \bar{N}_1 = \tfrac{5}{6}\xi(\xi - \sqrt{\tfrac{3}{5}}), \quad \bar{N}_2 = -\tfrac{5}{3}(\xi - \sqrt{\tfrac{3}{5}})(\xi + \sqrt{\tfrac{3}{5}}), \bar{N}_3 = \tfrac{5}{6}\xi(\xi + \sqrt{\tfrac{3}{5}}).
\end{aligned}
\tag{40}
$$

One can observe that these polynomials are of one order less than those used to interpolate the displacement unknowns.

B Fundamental nuclei of the stiffness matrix for MITC curved beam elements

The explicit expressions of the components of the 3×3 fundamental nuclei $K_{CC}^{\tau\varsigma ij}$, $K_{C\Omega}^{\tau\varsigma ij}$, $K_{\Omega C}^{\tau\varsigma ij}$ and $K_{\Omega\Omega}^{\tau\varsigma ij}$ are provided in the following. According to the introduced notation, the component 1 corresponds to the stiffness terms in direction s, 2 in ξ and 3 in η.

$$
\begin{aligned}
K_{CC}^{\tau\varsigma ij}(1,1) &= I_{\bar{i},s\bar{j},s} E^{11}_{\tau\varsigma\frac{1}{H}} + I_{\overline{ij}} \left(E^{55}_{\tau,\eta\varsigma,\eta H} + E^{66}_{\tau,\xi\varsigma,\xi H} \right) + \kappa I_{\overline{ij}} \left(E^{66}_{\tau\varsigma,\xi} + E^{66}_{\tau,\xi\varsigma} \right) + \kappa^2 I_{\overline{ij}} E^{66}_{\tau\varsigma\frac{1}{H}}, \\
K_{CC}^{\tau\varsigma ij}(1,2) &= I_{\bar{i},s\bar{j}} E^{66}_{\tau\varsigma,\xi} + \kappa \left(I_{\bar{i},s\bar{j}} E^{66}_{\tau\varsigma\frac{1}{H}} - I_{\overline{ij},s} E^{11}_{\tau\varsigma\frac{1}{H}} \right) \\
K_{CC}^{\tau\varsigma ij}(1,3) &= I_{\bar{i},s\bar{j}} E^{55}_{\tau\varsigma,\eta}, \\
K_{CC}^{\tau\varsigma ij}(2,1) &= +I_{\overline{ij},s} E^{66}_{\tau,\xi\varsigma} + \kappa \left(I_{\overline{ij},s} E^{66}_{\tau\varsigma\frac{1}{H}} - I_{\bar{i},s\bar{j}} E^{11}_{\tau\varsigma\frac{1}{H}} \right), \\
K_{CC}^{\tau\varsigma ij}(2,2) &= I_{\bar{i},s\bar{j},s} E^{66}_{\tau\varsigma\frac{1}{H}} + \kappa^2 I_{\overline{ij}} E^{11}_{\tau\varsigma\frac{1}{H}}, \\
K_{CC}^{\tau\varsigma ij}(2,3) &= 0, \\
K_{CC}^{\tau\varsigma ij}(3,1) &= I_{\overline{ij},s} E^{55}_{\tau,\eta\varsigma}, \\
K_{CC}^{\tau\varsigma ij}(3,2) &= 0, \\
K_{CC}^{\tau\varsigma ij}(3,3) &= I_{\bar{i},s\bar{j},s} E^{55}_{\tau\varsigma\frac{1}{H}},
\end{aligned}
\tag{41}
$$

$$
\begin{aligned}
K_{C\Omega}^{\tau\varsigma ij}(1,1) &= 0, \\
K_{C\Omega}^{\tau\varsigma ij}(1,2) &= I_{\bar{ij},s} E^{12}_{\tau,\xi\varsigma}, \\
K_{C\Omega}^{\tau\varsigma ij}(1,3) &= I_{\bar{ij},s} E^{13}_{\tau,\eta\varsigma}, \\
K_{C\Omega}^{\tau\varsigma ij}(2,1) &= 0, \\
K_{C\Omega}^{\tau\varsigma ij}(2,2) &= -\kappa I_{\bar{ij}} E^{12}_{\tau\varsigma,\xi}, \\
K_{C\Omega}^{\tau\varsigma ij}(2,3) &= -\kappa I_{\bar{ij}} E^{13}_{\tau,\eta\varsigma}, \\
K_{C\Omega}^{\tau\varsigma ij}(3,1) &= 0, \qquad K_{C\Omega}^{\tau\varsigma ij}(3,2) = 0, \qquad K_{C\Omega}^{\tau\varsigma ij}(3,3) = 0
\end{aligned}
\tag{42}
$$

$$
\begin{aligned}
&K^{\tau\varsigma ij}_{\Omega C}(1,1)=0, \qquad K^{\tau\varsigma ij}_{\Omega C}(1,2)=0, \qquad K^{\tau\varsigma ij}_{\Omega C}(1,3)=0,\\
&K^{\tau\varsigma ij}_{\Omega C}(2,1)=I_{\bar{i}_{,s}j}E^{12}_{\tau\varsigma,\xi},\\
&K^{\tau\varsigma ij}_{\Omega C}(2,2)=-\kappa I_{i\bar{j}}E^{12}_{\tau,\xi\varsigma},\\
&K^{\tau\varsigma ij}_{\Omega C}(2,3)=0,\\
&K^{\tau\varsigma ij}_{\Omega C}(3,1)=I_{\bar{i}_{,s}j}E^{13}_{\tau\varsigma,\eta},\\
&K^{\tau\varsigma ij}_{\Omega C}(3,2)=-\kappa I_{i\bar{j}}E^{13}_{\tau\varsigma,\eta},\\
&K^{\tau\varsigma ij}_{\Omega C}(3,3)=0,
\end{aligned}
\tag{43}
$$

$$
\begin{aligned}
&K^{\tau\varsigma ij}_{\Omega\Omega}(1,1)=0, \qquad K^{\tau\varsigma ij}_{\Omega\Omega}(1,2)=0, \qquad K^{\tau\varsigma ij}_{\Omega\Omega}(1,3)=0, \qquad K^{\tau\varsigma ij}_{\Omega\Omega}(2,1)=0,\\
&K^{\tau\varsigma ij}_{\Omega\Omega}(2,2)=I_{ij}\left(E^{22}_{\tau,\xi\varsigma,\xi H}+E^{44}_{\tau,\eta\varsigma,\eta H}\right),\\
&K^{\tau\varsigma ij}_{\Omega\Omega}(2,3)=I_{ij}\left(E^{23}_{\tau,\eta\varsigma,\xi H}+E^{44}_{\tau,\xi\varsigma,\eta H}\right),\\
&K^{\tau\varsigma ij}_{\Omega\Omega}(3,1)=0,\\
&K^{\tau\varsigma ij}_{\Omega\Omega}(3,2)=I_{ij}\left(E^{23}_{\tau,\xi\varsigma,\eta H}+E^{44}_{\tau,\eta\varsigma,\xi H}\right),\\
&K^{\tau\varsigma ij}_{\Omega\Omega}(3,3)=I_{ij}\left(E^{33}_{\tau,\eta\varsigma,\eta H}+E^{44}_{\tau,\xi\varsigma,\xi H}\right),
\end{aligned}
\tag{44}
$$

where the I terms correspond to the integrals of the shape functions along the beam axis, written as follows:

$$
\begin{aligned}
I_{i_{(,s)}j_{(,s)}} &= \int_l N_{i_{(,s)}} N_{j_{(,s)}}\ ds,\\
I_{\bar{i}_{(,s)}j_{(,s)}} &= \int_l \overline{N}_m N_{i_{(,s)m}} N_{j_{(,s)}}\ ds,\\
I_{i_{(,s)}\bar{j}_{(,s)}} &= \int_l N_{i_{(,s)}} \overline{N}_n N_{j_{(,s)n}}\ ds,\\
I_{\bar{i}_{(,s)}\bar{j}_{(,s)}} &= \int_l \overline{N}_m N_{i_{(,s)m}} \overline{N}_n N_{j_{(,s)n}}\ ds.
\end{aligned}
\tag{45}
$$

The subscripts i and j refer to the shape functions of the beam element, whereas m and n refer to the assumed strains. Accordingly, $N^m_{i_{(,s)}}$ is the i-th shape function (or its derivative) evaluated at the m-th tying point T_m:

$$
N_{i_{(,s)m}} = N_{i_{(,s)}}\left(T_m\right). \tag{46}
$$

On the other hand, the E terms correspond to the integrals of the expansion functions

over the cross-section. For instance:

$$
\begin{aligned}
E^{12}_{\tau,\xi\varsigma} &= \int_{\Omega} C_{12}\, F_{\tau,\xi} F_{\varsigma}\; d\xi\; d\eta, \\
E^{44}_{\tau,\eta\varsigma,\eta H} &= \int_{\Omega} C_{44}\, F_{\tau,\eta} F_{\varsigma,\eta}\; H\; d\xi\; d\eta, \\
E^{11}_{\tau\varsigma\frac{1}{H}} &= \int_{\Omega} C_{11}\, F_{\tau} F_{\varsigma}\; \frac{1}{H}\; d\xi\; d\eta.
\end{aligned}
\tag{47}
$$

When considering different fibre orientation angles, the material coefficients involved in the previous expression must be rotated according to the affine transformation of fourth order elasticity-like tensors, as shown in [**?**]. Full Gaussian quadrature is used for the numerical integrals in all cases.

It is worthy noting that the metric tensor, H, can be evaluated in the cross-sectional integrals only when the curvature, κ, along the length of the beam element is constant, see Eq. (**??**). If the curvature varies along s, i.e. $\kappa(s)$, 3D integrals must be computed over the volume.

References

[1] A. E. H. Love. The small free vibrations and deformation of a thin elastic shell. *Philosophical Transactions of the Royal Society of London. A*, 179:491–546, 1888.

[2] H. Lamb. On the deformation of an elastic shell. *Proceedings of the London Mathematical Society*, s1-21(1):119–146, 1889.

[3] J.L. Ericksen and C. Truesdell. Exact theory of stress and strain in rods and shells. *Archive for Rational Mechanics and Analysis*, 1(1):295 – 323.

[4] K. Washizu. Some considerations on a naturally curved and twisted slender beam. *Journal of Mathematics and Physics*, 43(1-4):111–116, 1964.

[5] E. Reissner. On one-dimensional large-displacement finite-strain beam theory. *Studies in Applied Mathematics*, 52(2):87–95, 1973.

[6] D.G. Ashwell and R. H. Gallagher. *Finite element for thin shells and curved members*. Willey, London, 1976.

[7] M.R. Banan, G. Karami, and M. Farshad. Finite element analysis of curved beams on elastic foundations. *Computers & Structures*, 32(1):45 – 53, 1989.

[8] E. Tufekci and A. Arpaci. Analytical solutions of in-plane static problems for non-uniform curved beams including axial and shear deformations. *Structural Engineering & Mechanics*, 22(2):131 – 150, 2006.

[9] A. K. Noor and J. M. Peters. Mixed models and reduced/selective integration displacement models for nonlinear analysis of curved beams. *International Journal for Numerical Methods in Engineering*, 17(4):615–631, 1981.

[10] H. Stolarski and T. Belytschko. Membrane locking and reduced integration for curved elements. *Journal of Applied Mechanics*, 49(1):172 – 176, 1982.

[11] D.J. Dawe. Numerical studies using circular arch finite elements. *Computers & Structures*, 4(4):729 – 740, 1974.

[12] C. R. Babu and G. Prathap. A linear thick curved beam element. *International Journal for Numerical Methods in Engineering*, 23(7):1313–1328, 1986.

[13] S. N. Atluri, M. Iura, and S. Vasudevan. A consistent theory of finite stretches and finite rotations, in space-curved beams of arbitrary cross-section. *Computational Mechanics*, 27(4):271–281, Apr 2001.

[14] A. Tessler and L. Spiridigliozzi. Curved beam elements with penalty relaxation. *International Journal for Numerical Methods in Engineering*, 23(12):2245–2262, 1986.

[15] I. Fried. Shape functions and the accuracy of arch finite elements. *AIAA Journal*, 11(3):287 – 291.

[16] J. G. Kim and Y. Y. Kim. A new higher-order hybrid-mixed curved beam element. *International Journal for Numerical Methods in Engineering*, 43(5):925–940, 1998.

[17] E.N. Dvorkin and K.J. Bathe. A continuum mechanics based four-node shell element for general non-linear analysis. *Engineering Computations*, 1(1):77–88, 1984.

[18] R.H. MacNeal. Derivation of element stiffness matrices by assumed strain distributions. *Nuclear Engineering and Design*, 70(1):3 – 12, 1982.

[19] M.L. Bucalem and K.-J. Bathe. Higher-order MITC general shell elements. *International Journal for Numerical Methods in Engineering*, 36(21):3729–3754, 1993.

[20] H. C. Huang and E. Hinton. A new nine node degenerated shell element with enhanced membrane and shear interpolation. *International Journal for Numerical Methods in Engineering*, 22(1):73–92, 1986.

[21] K.C. Park and G.M. Stanley. A curved C^0 shell element based on assumed natural-coordinate strains. *Journal of Applied Mechanics*, 53(2):278–290, 1986.

[22] J. Jang and P.M. Pinsky. An assumed covariant strain based 9-node shell element. *International Journal for Numerical Methods in Engineering*, 24(12):2389–2411, 1987.

[23] M. Cinefra, C. Chinosi, and L. Della Croce. MITC9 shell elements based on refined theories for the analysis of isotropic cylindrical structures. *Mechanics of Advanced Materials and Structures*, 20(2):91–100, 2013.

[24] E. Carrera, A. G. de Miguel, and A. Pagani. Extension of MITC to higher-order beam models and shear locking analysis for compact, thin-walled, and composite structures. *International Journal for Numerical Methods in Engineering*, 112(13):1889–1908, 2017.

[25] S.G. Lekhniskii. *Anisotropic plates*. Gordon & Breach, New York, 1968. translated from 2nd russian Edition by S.W. Tsai and T. Cheron.

[26] N.J. Pagano. Exact solutions for composite laminates in cylindrical bending. *Journal of Composite Materials*, 3(3):398–411, 1969.

[27] T.K. Varadan and K. Bhaskar. Bending of laminated orthotropic cylindrical shellsan elasticity approach. *Composite Structures*, 17(2):141 – 156, 1991.

[28] R.K. Kapania and S. Raciti. Recent advances in analysis of laminated beams and plates, part I: Shear effects and buckling. *AIAA Journal*, 27(7):923–935, 1989.

[29] M. Hajianmaleki and Mohamad S. Q. Vibrations of straight and curved composite beams: A review. *Composite Structures*, 100(Supplement C):218 – 232, 2013.

[30] J. N. Reddy. *Mechanics of laminated composite plates and shells. Theory and Analysis*. CRC Press, 2^{nd} edition, 2004.

[31] R. P. Shimpi and Y. M. Ghugal. A new layerwise trigonometric shear deformation theory for two-layered cross-ply beams. *Composites Science and Technology*, 61(9):1271 – 1283, 2001.

[32] M. Tahani. Analysis of laminated composite beams using layerwise displacement theories. *Composite Structures*, 79(4):535 – 547, 2007.

[33] A. J. M. Ferreira. Analysis of composite plates using a layerwise theory and multiquadrics discretization. *Mechanics of Advanced Materials and Structures*, 12(2):99–112, 2005.

[34] E. Carrera, A. Pagani, M. Petrolo, and E. Zappino. Recent developments on refined theories for beams with applications. *Mechanical Engineering Reviews*, 2(2):1–30, 2015.

[35] E. Carrera, M. Cinefra, E. Zappino, and M. Petrolo. *Finite Element Analysis of Structures Through Unified Formulation*. John Wiley and Sons, Ltd, 2014.

[36] A. Pagani, A.G. de Miguel, M. Petrolo, and E. Carrera. Analysis of laminated beams via unified formulation and Legendre polynomial expansions. *Composite Structures*, 156:78 – 92, 2016.

[37] E. Carrera, M. Maiarù, and M. Petrolo. Component-wise analysis of laminated anisotropic composites. *International Journal of Solids and Structures*, 49:1839–1851, 2012.

[38] D. Chapelle and K.J. Bathe. *The finite elemente analysis of shells - Fundamentals*. Springer, Berlin, 2003.

[39] R. M. Jones. *Mechanics of composite materials*. Taylor and Francis Ltd., London, UK, 2^{nd} edition, 1998.

[40] E. Carrera, A.G. de Miguel, and A. Pagani. Hierarchical one-dimensional finite elements based on legendre polynomial expansions. *International Journal of Mechanical Sciences*, 120:286 – 900, 2017.

[41] B. Szabó and I. Babuška. *Finite Element Analysis*. John Wiley and Sons, Ltd, 1991.

[42] A. Pagani, A.G. de Miguel, and E. Carrera. Component-wise analysis of laminated structures by hierarchical refined models with mapping features and enhanced accuracy at layer to fiber-matrix scales. *Mechanics of Advanced Materials and Structures*, 2017. In Press.

[43] KJ. Bathe. *Finite element procedures*. Upper Saddle River, New Jersey: Prentice Hall, 1996.

[44] J. Barlow. Optimal stress locations in finite element models. *International Journal for Numerical Methods in Engineering*, 10(2):243–251, 1976.

[45] G. De Pietro, A.G. de Miguel, E. Carrera, G. Giunta, S. Belouettar, and A. Pagani. Strong and weak form solutions of curved beams via carreras unified formulation. 2017. Submitted.

[46] R.H. Macneal and R.L. Harder. A proposed standard set of problems to test finite element accuracy. *Finite Elements in Analysis and Design*, 1(1):3 – 20, 1985.

[47] K.S. Surana and S.H. Nguyen. Two-dimensional curved beam element with higher-order hierarchical transverse approximation for laminated composites. *Computers & Structures*, 36(3):499–511, 1990.

[48] A.S. Kaddour and M.J. Hinton. Input data for test cases used in benchmarking triaxial failure theories of composites. *Journal of Composite Materials*, 46(19-20):2295–2312, 2012.